Review

Polyglycerol Systems in Additive Manufacturing: Structure, Properties, and Processing

Julie Pearl M. Andal , Roxanne R. Navarro , Reymark D. Maalihan *

Posted Date: 18 August 2025

doi: 10.20944/preprints202506.1354.v2

Keywords: polyglycerol; additive manufacturing; thermal stability; mechanical performance; crosslinking; shape memory polymers

Review

Polyglycerol Systems in Additive Manufacturing: Structure, Properties, and Processing

Julie Pearl M. Andal [1], Roxanne R. Navarro [2] and Reymark D. Maalihan [3,*]

[1] College of Engineering and College of Engineering Technology, Batangas State University, Alangilan Campus, Batangas City, 4200 Philippines

[2] College of Engineering, Batangas State University, Alangilan Campus, Batangas City, 4200 Philippines

[3] Department of Coatings and Polymeric Materials, North Dakota State University, Fargo, North Dakota 58102 United States

* Correspondence: reymark.maalihan@ndsu.edu or reymark.maalihan21@gmail.com

Abstract

Additive manufacturing (AM) demands materials that combine precise printability with reliable thermal and mechanical performance. Polyglycerol (PG)-based macromolecular systems offer exceptional tunability through controlled architecture and chemical modification, enabling their use across both light-based and extrusion AM platforms. Strategic enhancements such as chemical functionalization, network formation, and hybrid reinforcement have expanded their capabilities from biomedical to structural applications, delivering improved stability, strength, and functionality. Despite these advances, performance-processing trade-offs and dispersion challenges remain barriers to widespread adoption. This review synthesizes current knowledge on PG-based materials in AM, mapping key structure-property-processing relationships and identifying strategies to advance their development as versatile and sustainable options for next-generation manufacturing.

Keywords: polyglycerol; additive manufacturing; thermal stability; mechanical performance; crosslinking; shape memory polymers

1. Introduction

Additive manufacturing (AM), often known as 3D printing, enables the fabrication of tailored polymer components with enhanced material efficiency and extended service life compared to conventional subtractive methods [1,2]. However, the structural reliability of many printed parts is often compromised by inadequate thermomechanical performance, which affects a material's ability to retain mechanical integrity throughout fabrication, post-processing, and end use [3,4]. This challenge is especially critical for structural AM components exposed to cyclic loading, temperature fluctuations, and long-term mechanical stress [5,6]. For example, conventional photo-activated resins used in vat-based AM often yield brittle, overly rigid components even after post-curing, or soft ones with low glass transition temperatures (T_g), making them unsuitable for load-bearing use [7,8]. Although low T_g limits structural performance, it can be advantageous in soft AM applications such as shape memory systems and 4D printing, where thermal responsiveness and programmed shape transformation are essential [9].

Polyglycerol (PG)-based macromolecular systems are increasingly explored as versatile materials in AM, owing to their tunable chemical architecture and high functional density [10–12]. This review surveys PG-based structures, including linear, hyperbranched, and dendritic forms, and emphasizes their transition from predominantly biomedical roles to broader industrial and structural applications. Representative materials such as poly(glycerol sebacate) (PGS), poly(glycerol sebacate acrylate) (PGSA), polyglycerol diacrylate (PGDA), and poly(glycerol dodecanedioate) (PGD) are assessed for their compatibility with AM techniques. The polyhydroxylated backbone of PG allows for precise tuning of crosslinking, branching, and hydrophilicity, supporting their application across

Peer-reviewed version available at Macromol 2025, 5, 48; doi:https://doi.org/10.3390/macromol5040048

stereolithography (SLA), digital light processing (DLP), volumetric AM (VAM), and, with suitable modifications, fused deposition modeling (FDM). In these platforms, the interplay of rheological, photochemical, and mechanical characteristics directly influences both print resolution and final part performance. As AM advances toward more demanding load-bearing and multifunctional applications, interest is shifting toward materials that balance printability with enhanced thermomechanical stability. While PG-based systems have been extensively studied in biomedical settings, their broader potential in high-performance industrial AM remains underexplored. This review aims to bring that emerging opportunity into focus.

To overcome thermomechanical limitations in PG-based systems, strategic chemical modifications have proven effective. Acrylated PGs with carbon nanotubes (CNTs) show enhanced cross-linking, stiffness, and thermal stability while maintaining excellent DLP printability [13]. Natural fillers like corn-derived protein, crosslinked into the PGS backbone, improve anisotropic mechanics resembling native myocardium [14]. Blending PGS with polycaprolactone (PCL) and bioactive glass (BG) microspheres enhances stiffness, controls degradation, and boosts biocompatibility [15]. Similarly, acrylating PGD into photocurable resin enables rapid UV crosslinking, lowers crystallinity, and tunes thermal transitions near body temperature [16]. These changes preserve shape memory behavior and support 3D printing with improved mechanical consistency and biocompatibility for soft tissue repair.

This review provides an in-depth analysis of PG-based polymer systems for AM, emphasizing their thermomechanical properties. It explores structure-property relationships, thermal stability, and mechanical behavior in printed forms, and outlines strategies to enhance both structural and functional performance. The review also offers a critical assessment of current limitations and future directions for integrating PG-based materials into next-generation AM technology.

2. Structure-Property Relationships in a PG System

PG exists in linear (LPG), hyperbranched (HPG), and dendritic (DPG) forms, each offering distinct thermal and mechanical characteristics due to differences in molecular topology. LPG, with its flexible backbone and uniformly spaced hydroxyl groups, supports efficient chemical modification and demonstrates a broad T_g range (–18.5 to –28.3 °C), particularly in copolymerized forms [17]. It also achieves moderate mechanical strength (0.2 to 5.0 MPa) at high molecular weights (MWs) due to chain entanglement and hydrogen bonding [18–21]. These features support low-temperature melt extrusion printing and molding. HPG and DPG, characterized by dense terminal hydroxyl groups and highly branched, compact architectures (degree of branching (DB): 0.60–0.63 and 0.50–0.70), offer improved aqueous solubility, chemical functionalization potential, and greater thermal stability, making them suited for reactive resin-based 3D printing methods (e.g., SLA, DLP) [22,23]. However, limited chain entanglement leads to reduced mechanical strength (HPG ~1.6 MPa) [21,23–25], which can be mitigated via crosslinking strategies. DPG provides improved mechanical performance (~3.0–10.0 MPa) when integrated into composite systems (e.g., 15–25 wt% in soy protein isolate films), along with a T_g range of –14 to –20 °C [26,27]. These structure-property relationships, governed by DB, MW, and terminal group functionality, are crucial for tuning PGs for 3D printable formulations used in drug delivery devices, soft coatings, and nanocomposite scaffolds. Table 1 summarizes key thermal and mechanical metrics across PG architectures.

Peer-reviewed version available at Macromol 2025, 5, 48; doi:https://doi.org/10.3390/macromol5040048

Table 1. Structural influence on thermal and mechanical properties of PG architectures.

Property	LPG	HPG	DPG
DB	~0 [28]	0.60–0.63 (methacrylated) [23]	0.50–0.70 [22]
T_g	–30.0 to 30.0 °C (PGS-co-diacids) [17]	–39 °C [23]	–14 to –20 °C (PG-succinate) [27]
Tensile strength	0.2 to 5.0 MPa (PGS) [18]	1.6 ± 0.4 MPa [23]	~3.0–10.0 MPa (at 15 to 25 wt% in soy protein isolate films) [26]

2.1. Synthetic Pathways and Architectural Engineering of PGs

The structural versatility of PGs stems from their tunable architectures, which can be precisely engineered through advanced polymerization strategies. LPGs are synthesized via anionic ring-opening polymerization (AROP) using alkoxide initiators, which provide control over MW and dispersity to yield uniform chains suitable for predictable behavior and dense packing [29]. HPGs and DPGs are obtained through strategies that allow fine-tuned branching. Reversible addition-fragmentation chain transfer (RAFT) polymerization enables hyperbranched architectures with controllable branching density and functional end-groups [30]. In contrast, copper-catalyzed azide-alkyne cycloaddition (CuAAC) "click" chemistry offers a modular route to defect-free, highly ordered dendritic structures [31]. Atom transfer radical polymerization (ATRP) further enhances structural control, enabling precise placement of functional groups and hybrid architectures [32,33].

The architectural scope of PGs has expanded to include bottlebrush, comb, and star-brush topologies, typically constructed via grafting-from or grafting-through methods, often RAFT-mediated. Core polymer architecture, whether linear, cyclic, or multifunctional, strongly influences molecular folding, packing, and performance across scales. For instance, multifunctional initiators facilitate star-shaped structures, while backbone grafting yields comb polymers with tunable side-chain density [34,35]. Side-chain engineering at the monomer level adds further design flexibility. Incorporating alkyl glycidyl ethers (e.g., butyl glycidyl ether) introduces dynamic, apolar side chains that disrupt hydrogen bonding, increase free volume, lower the T_g, and enhance chain mobility [36]. Similarly, carboxyethyl-functionalized monomers, such as 4-acryloylamino-4-(carboxyethyl)heptanedioic acid, introduce ionizable groups that enable responsiveness to pH and ionic environments. DPG, when incorporated into nanogels, improves colloidal stability and supports self-assembly [37].

These architectural and compositional strategies directly affect nanostructure formation and phase behavior. Block copolymers synthesized by sequential monomer addition undergo microphase separation, forming self-assembled nanostructures that alter surface morphology, chemical functionality, and interactions with biological agents like proteins [38]. Hyperbranched-linear block copolymers integrate the solubility and processability of hyperbranched segments with the thermal tunability and structural precision of linear chains, making them ideal for stimuli-responsive biomedical materials [39]. Lastly, random copolymers of HPG with redox-responsive monomers such as 1,4,5-oxadithiepan-2-one exhibit uniform architectures that support well-defined nanoparticle formation and thermal stability. Increasing disulfide content elevates T_g and introduces emerging crystallinity, enabling precise material tuning [40].

Peer-reviewed version available at *Macromol* **2025**, *5*, 48; doi:https://doi.org/10.3390/macromol5040048

2.2. Influence of Molecular Weight, Branching, and Functional Groups on the Mechanical and Interfacial Properties of PGs

Both HPG and LPG architectures offer tunable platforms for controlling the mechanical and interfacial properties of amphiphilic copolymers. MW, DB, and functional group identity govern phase morphology, wettability, and viscoelastic behavior, key parameters in applications like surface coatings and AM [41]. In polydimethylsiloxane (PDMS)-HPG copolymers, increasing PDMS block size from 1k to 10k Da and adjusting glycidol:PDMS ratios (e.g., 10:1 to 20:1) enhances phase segregation and mechanical toughness. Systems with 5k or 10k PDMS blocks and moderate HPG branching (e.g., 10:1 or 15:1) form stratified domains that resist fouling through reduced bioadhesion and improved energy dissipation [42]. The branching structure of HPG significantly affects rheology. DB values between 0.17 and 0.58, tuned via ethoxyethyl glycidyl ether comonomer incorporation, allow precise control over viscosity and flow behavior. Lower DB increases chain flexibility and reduces intermolecular interactions, while higher DB leads to denser architectures with stronger intramolecular hydrogen bonding and elastic response [43]. LPG systems offer complementary control through side-chain functionalization. LPG-based block copolymers (e.g., 9/1 and 1/1 blocks, ~10.1 and ~7.1 kDa, respectively) were designed bearing catechol and fluoroalkyl groups [44]. Longer LPG blocks formed smooth, hydrophilic coatings (~60° contact angle), while shorter, highly functionalized variants produced rougher, micellar structures. On polytetrafluoroethylene, contact angles varied from 129 ± 10° to below 65°, depending on aggregation and surface alignment of fluoroalkyl chains.

2.3. Strategies to Enhance Mechanical Strength: Crosslinking, Copolymerization, and Filler Addition

Improving the mechanical performance of PG-based polymers for potential AM use relies on three principal strategies: crosslinking, copolymerization, and filler incorporation. Each approach enhances stiffness and durability in distinct ways but requires trade-offs in flexibility, biocompatibility, and processing compatibility.

Crosslinking enhances rigidity and thermal stability by forming covalent or supramolecular networks within the PG matrix [18,45]. Various crosslinkers, including ethylene glycol diglycidyl ether (EGDGE), divinyl sulfone (DVS), glutaraldehyde (GA), 1,11-di(mesyloxy)-3,6,9-trioxaundecane (TEG-Ms_2), and 1,11-dibromo-3,6,9-trioxaundecane (TEG-Br_2), have been evaluated [46]. While EGDGE and DVS produced freestanding membranes with improved modulus, they also altered surface properties, increasing protein and bacterial adhesion in some cases. Over-crosslinking with agents like DVS and TEG derivatives raised stiffness but reduced elasticity and transferability. Inconsistent optimal curing conditions, ranging from acidic aqueous reactions to high-temperature protocols, complicate standardization. These challenges highlight the need for predictive models to guide crosslinker selection based on mechanical and biological performance targets.

Copolymerization allows fine-tuning of thermomechanical behavior by adjusting monomer composition [47]. For instance, increasing glycidyl methyl ether (GME) content in LPG chains led to a five-decade reduction in zero-shear viscosity and a linear decrease in T_g, due to disrupted hydrogen bonding. While effective in modifying viscosity and T_g, the copolymer architecture is sensitive to synthesis methods [48]. Variations in comonomer distribution between copolymerization and post-polymerization modification impact reproducibility and performance consistency.

Filler incorporation strengthens PG-based scaffolds by introducing nanoscale reinforcements [24]. Saudi et al. (2022) demonstrated that electrospun PCL/PGS scaffolds loaded with 5-15 wt% nanohydroxyapatite (nHA) achieved a Young's modulus increase from 0.16 to 0.3 MPa, suitable for nerve tissue engineering [49]. PGS improved hydrophilicity and cell adhesion, enabling high nHA loadings without cytotoxic effects. However, at 15 wt%, particle agglomeration introduced risks of mechanical discontinuity. Other fillers, such as graphene or nanosilicates, offer higher stiffness gains but are often limited by cytotoxicity and dispersion issues [19,50].

Figure 1 compares crosslinking, copolymerization, and filler integration across four performance domains: mechanical reliability, long-term stability, biocompatibility, and thermal resilience. Scores,

Peer-reviewed version available at *Macromol* **2025**, *5*, 48; doi:https://doi.org/10.3390/macromol5040048

based on reported literature data [38,46,51–54], primarily from the past three years, were normalized to a 10-point scale. Crosslinking scores highest in mechanical reliability and long-term stability, reflecting its robustness and durability. Copolymerization also performs well in mechanical reliability and thermal stability, and shares the highest biocompatibility rating, but performs poorly in long-term stability, likely due to chain degradation or synthesis variability. Filler integration offers strong mechanical support and good biocompatibility, but lower scores in thermal resilience and long-term stability, likely due to filler dispersion or aggregation issues.

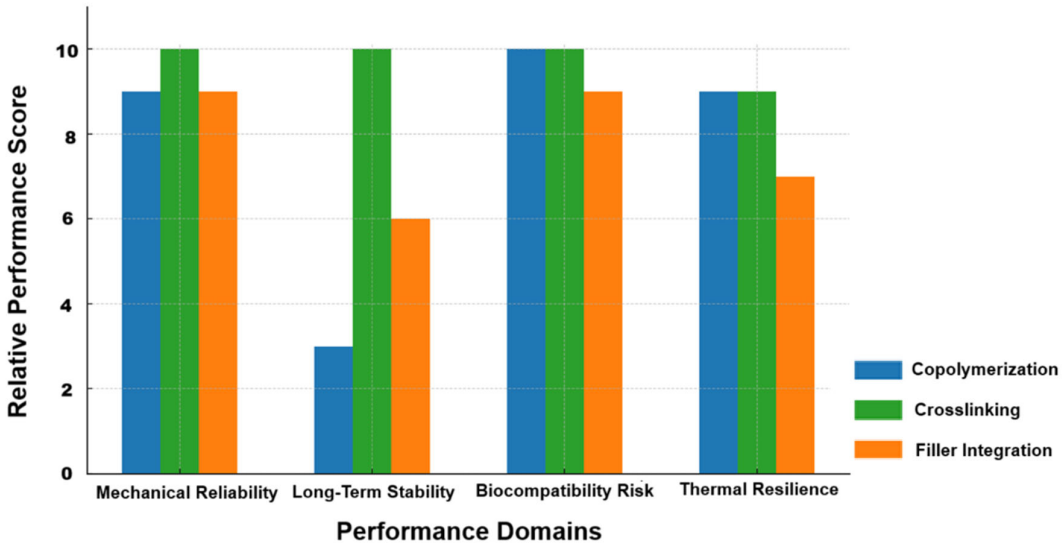

Figure 1. Stacked comparison of enhancement strategies across four performance domains in PG-based systems.

While each of these strategies offers valuable tools for tailoring PG-based material performance, they are typically implemented in isolation. However, the emerging frontier in AM involves combining these methods synergistically to create hybrid systems. Such systems integrate multiple fillers or polymer phases, offering enhanced mechanical, thermal, and structural properties beyond what single-strategy approaches can achieve. These advanced combinations are discussed in detail in Section 4.2.

3. Thermal Stability and Processing Considerations

PG-based polymers feature ether linkages in their backbone that confer inherent thermal stability. In HPG and DPG architectures, restricted chain mobility further enhances dimensional and thermal stability during processing. Structural modifications, such as the incorporation of aromatic or hydrophobic groups, can raise decomposition temperatures, broadening their suitability for high-temperature AM applications [54,55]. Thermoplastic derivatives of PGs can be engineered for precise melt-flow behavior compatible with extrusion-based techniques like FDM, while acrylated PGs serve as effective photocurable resins for SLA via efficient UV crosslinking [57,58]. Altogether, the tunable chemistry and favorable processing characteristics of PG-based polymers make them strong candidates for diverse high-performance AM applications.

3.1. Thermal Decomposition Profiles

Thermal stability is a critical property for polyglycerol-based materials used in AM, particularly in processes involving elevated temperatures during printing or post-processing. Compared to conventional thermoplastics like PLA and ABS, PG systems especially those with chemical

Peer-reviewed version available at *Macromol* **2025**, *5*, 48; doi:https://doi.org/10.3390/macromol5040048

crosslinking offer improved thermal resistance, including elevated T_g, melting points (T_m), and decomposition thresholds ($T_{10\%}$ and $T_{50\%}$) [59,60]. In SLA and other UV-curable platforms, crosslinked PG resins exhibit higher degradation onset temperatures due to dense covalent networks formed during curing, enhancing stability during subsequent thermal exposure [61,62]. Additional reinforcement with materials such as cellulose nanofibers, graphene oxide, or sodium silicate further raises decomposition temperatures and strengthens the overall matrix [63,64].

Table 1 summarizes the thermal properties of representative PG-based materials tailored for specific functions. Typically PGS has a T_g of –22.5 °C and a T_m of 5.6 °C, suitable for soft biomedical use [65]. Electrospinning with chitin-lignin raises its T_m to ~63 °C, likely due to enhanced hydrogen bonding and crystalline alignment, indicating suitability for wound care scaffold [66]. PG tartrate, reinforced with cellulose and nanosilica, achieves a T_{max} near 300 °C and a char yield of 59.5%, offering excellent thermal durability for environmental remediation. This is attributed to the dendritic fibrous nature of SiO_2, whose high surface area and hydroxyl-rich structure enhance cross-linking, porosity, and heat resistance within the resulting hydrogel matrix [67]. Methacrylated PG adipate, synthesized enzymatically, exhibits low T_g (–41 to –20 °C) and UV-curability, ideal for soft photopolymer applications [68]. A polyester polyol synthesized from glycerol acetate, coconut oil polyol, and phthalic anhydride displays a T_m around –12 °C and low crystallinity, aligning with the needs of sustainable polyurethane formulations. These properties stem from its high soft segment content and low hard segment content, which limit crystalline domain formation and enhance elasticity [69].

PGD exhibits shape memory and melting behavior near 35–42 °C, making it suitable for minimally invasive biomedical devices [70]. PGS-co-succinate copolymers show T_g values from –19 to +23 °C and T_{max} up to 400 °C. Increased succinate content enhances thermal stability and density, expanding their use in structural biomedical components [17]. HPG copolymers with aziridine show $T_{10\%}$ between 58–108 °C and $T_{50\%}$ up to 391 °C, with tunable crosslinking for waterborne adhesive applications. $T_{10\%}$ reflects the onset of decomposition, influenced by volatile compounds or low-MW fragments, while $T_{50\%}$ indicates deeper degradation, representing the core thermal stability of the cross-linked polymer [71].

Table 2. Thermal properties of PG-based macromolecular system.

PG-based material	Structural Modification / Formulation	T_g	T_m	T_{onset} / T_{max}	Char yield	Reference
PGS	Two-step synthesis with sebacic acid	–22.5	5.6			[65]
PGS	Electrospun chitin-lignin sol-gel		63			[66]
PG tartrate	Crosslinked with cellulose, reinforced with nanosilica and apple peel			T_{max} ~ 300	59.5	[67]
PG adipate - methacrylate	One-pot two-step enzymatic methacrylation	−41 to −20				[68]

PG polyester polyol	Glycerol acetate + coconut oil polyol + phthalic anhydride		−11.4 to −12.2	[69]
PGD	Varying curing time and temperature		35 to 42	[70]
PGS-co-succinate	Varying succinate content	-19 to 23	T_{max} ~ 400	[17]
Acrylic HPG	Copolymer with aziridine		$T_{10\%}$ = 58 to 108 $T_{50\%}$ =354 to 391	[71]

3.2. Suitability for High-Temperature AM Platforms

PGS exhibits thermal and rheological properties that limit its use in high-temperature extrusion-based AM. It softens and becomes rubbery at physiological temperatures (~37 °C), with melting transitions reported as low as 37 °C and thermal crosslinking temperatures ranging from 124–141 °C, making it thermally unstable under conventional melt-processing conditions [18,45]. FDM typically operates at 180–200 °C for processing thermoplastics like polylactic acid (PLA) and acrylonitrile butadiene styrene (ABS) [72,73]. Although FDM systems can be configured to operate at lower temperatures or accommodate certain low-melting materials, PLA and ABS still require elevated temperatures for proper extrusion. As such, native PGS due to its low viscosity, thermal instability, and weak mechanical integrity, remains incompatible with consistent melt extrusion. For example, attempts to fabricate PG-co-diacid sheets at 180 °C using twin-screw extrusion resulted in brittle or sticky products, and prepolymers synthesized via microwave methods failed to form viable filaments [74]. To overcome these challenges, chemical modification strategies such as acrylation, methacrylation, or norbornene functionalization have been employed to introduce polymerizable groups that support photopolymerization under mild conditions [75,76]. This enables a shift toward light-based AM platforms which are better suited for low-viscosity, photocurable resins. Ao-Ieong et al. (2021) demonstrated this approach by developing PGSA, a photocurable PGS derivative optimized for DLP [64]. Thermal post-curing of photocrosslinked PGSA at 120–160 °C significantly enhanced mechanical performance, doubling Young's modulus and tripling ultimate tensile strength, due to additional ester crosslinking between residual hydroxyl and carboxylic acid groups. Thermally treated PGSA also showed slower, surface erosion-based degradation and sustained high biocompatibility. Notably, these scaffolds retained mechanical stability after autoclave sterilization, confirming the robustness of the thermally crosslinked network for biomedical applications.

4. Mechanical Performance in 3D Printed Forms

The mechanical properties of 3D printed PG scaffolds are generally characterized through tensile and compressive responses. How the material performs under elongation versus compression is quantified by parameters such as Young's modulus, ultimate tensile strength (UTS), elongation at break, and compressive modulus [1,2]. While tensile and compressive properties represent distinct deformation modes and are not directly interchangeable, their combined evaluation defines the scaffold's functional mechanical range and informs material design for tissue-specific applications. One approach involves blending PGS-fumarate (PGSF), a UV-crosslinkable PGS derivative, with poly(ethylene glycol) diacrylate (PEGDA) [77]. This formulation allows extrusion-based 3D printing

Peer-reviewed version available at *Macromol* **2025**, *5*, 48; doi:https://doi.org/10.3390/macromol5040048

with in situ photopolymerization, resulting in soft yet robust scaffolds. Rectangular tensile specimens (40 mm × 5 mm × 0.8 mm) exhibited Young's moduli from 1.31 to 3.12 MPa, with higher UV intensity and slower print speeds increasing crosslink density, and thus stiffness, due to PEGDA's inherent rigidity. UTS ranged from 0.07 to 0.43 MPa, while strain at failure declined from 20% to 7%, consistent with a brittle, linear-elastic response. In contrast to native PG, which features a lower modulus (0.056–1.2 MPa) and can deform up to 448%, the composites showed significantly increased stiffness at the expense of flexibility. This highlights the typical trade-off introduced by photopolymer crosslinking.

To further expand mechanical tunability, PGSA-co-hydroxyethyl methacrylate (HEMA) copolymers have been developed using DLP printing [78]. These materials enabled high-resolution scaffold fabrication with minimal shrinkage (~4.9%) and composition-driven mechanical control. PGSA50-PHEMA50 formulation exhibited the highest tensile strength (15.6 MPa), while PGSA60-PHEMA40 showed the greatest elongation at break (46.95%), illustrating the expected stiffness-ductility trade-off in acrylate copolymers. After 8 weeks in phosphate-buffered saline (PBS), these constructs retained mechanical functionality, validating their role as temporary implants during early tissue healing.

Complementary efforts to enhance compressive properties have involved reinforcing PG scaffolds with a collagen type I/II–hyaluronic acid (CI/II–HyA) matrix [10]. Under dry conditions, the composite exhibited a compressive modulus of 167.0 kPa. Such is more than twice that of PG alone (80.0 kPa) due to the structural reinforcement of collagen. The CI/II-HyA matrix by itself was mechanically weak (10.8 kPa), underscoring the benefit of composite synergy. In hydrated conditions, modulus values decreased (45.2 kPa for the composite vs. 35.7 kPa for PG), reflecting water-induced softening. Despite this, the reinforced scaffold maintained superior compressive stiffness. These constructs also remained mechanically stable during a four-week in vitro degradation period, gradually softening in a biologically compatible manner, making them suitable for early-stage cartilage regeneration.

4.1. Influence of Printing Parameters on Anisotropy and Layer Bonding

The anisotropic mechanical behavior and interlayer cohesion of PGS-based scaffolds are strongly influenced by printing parameters such as material formulation, deposition technique, and structural orientation. While conventional FDM operates at temperatures that exceed the thermal stability limits of unmodified PGS, anisotropy can still be achieved through alternative low-temperature fabrication methods, including solvent-assisted extrusion and electrospinning, that avoid thermal degradation. By carefully tuning these variables, PGS constructs can be fabricated that closely replicate the direction-dependent properties of native soft tissues, especially in cardiac and valvular applications.

In extrusion-based printing, anisotropy is commonly achieved by alternating strand orientations across printed layers [79]. Ruther et al. (2022) demonstrated this by combining PGS with zein and NaCl to formulate a printable ink suitable for room-temperature extrusion [14]. The filament orientation induced significant directional dependence in mechanical properties. Specifically, scaffolds containing 30 wt% zein displayed a dry-state Young's modulus of 29 ± 2 MPa and UTS of 1400 ± 141 kPa, with elongation at break limited to 21 ± 3%. Upon hydration, these values decreased to 342 ± 87 kPa (modulus) and 272 ± 83 kPa (UTS), while the strain at break nearly doubled to 51 ± 7%. This softening was attributed to water-induced plasticization of zein, which lowers its T_g and enhances molecular flexibility. Layer bonding in these scaffolds benefited from the inclusion of sieved NaCl, which was partially dissolved during printing in ethanol and later leached to create micropores approximately 15 ± 7 μm in size. These pores increased the interfacial surface area, promoting mechanical interlocking between layers. Print fidelity was quantified using a combined metric (P_r), incorporating filament spreading ratio and pore geometry. Values close to 1.05 indicated highly stable and dimensionally accurate prints, particularly at optimal PGS-zein to salt ratios between 1:2 and 1:3 by weight.

Peer-reviewed version available at *Macromol* **2025**, *5*, 48; doi:https://doi.org/10.3390/macromol5040048

In contrast, Gürbüz et al. (2024) induced anisotropy at the nanoscale using electrospinning to fabricate radially aligned PCL/PGS/polysulfone (PSf) nanofibrous scaffolds [80]. Using a 3D-printed centered-pillar mold, they achieved radial fiber alignment that mimicked the ventricularis layer of native valve leaflets. The fibers guided human umbilical vein endothelial cell alignment and elongation, illustrating the biological impact of topographical anisotropy. Fiber diameters ranged from 450 to 650 nm, with minimal variation across the mat. Key electrospinning parameters, including a flow rate of 0.1 mL h^{-1}, voltage of 30 kV, and a 12 cm collection distance, were optimized to ensure uniform deposition. Solution properties were equally important. The addition of PSf increased conductivity to 0.371 μS cm^{-1} and reduced intrinsic viscosity from 5.98 to 0.72 dL g^{-1}. This facilitated thinner fibers and tighter entanglement. Unlike extrusion printing, electrospinning generated a seamless fibrous network without discrete layers. This structural continuity reduced the risk of delamination and improved overall mat integrity.

Although the two approaches differ in method and scale, both successfully engineered anisotropy and strong interfacial bonding through careful control of formulation and deposition, while avoiding the high thermal loads of FDM. The extrusion method enables tunable mechanical gradients through filament design and curing dynamics. In contrast, electrospinning provides nanoscale architectural control and promotes biologically relevant cell alignment.

4.2. Hybrid Reinforcements

Building on the principles outlined in Section 2.3, hybrid reinforcement strategies integrate multiple strengthening mechanisms, such as combining organic and inorganic phases, embedding nanoscale fillers, and incorporating polymer-polymer composite systems to achieve multifunctional performance in AM. These approaches enhance stiffness, toughness, functionality, and sustainability by exploiting complementary material attributes.

Organic-inorganic hybrids exemplify this synergy. A PG-based polyurethane-waterglass adhesive achieved compressive strengths above 50 MPa in 2 h and ~76 MPa at full cure [81]. Its three-dimensional interpenetrating network (3D-IPN) consists of amorphous polyurethane and crystalline polysilicic acid/$NaHCO_3$, with ~12 μm silicate spheres chemically anchored via Si–O–C linkages. The rigid inorganic phase bears load, while the ductile matrix dissipates stress, as confirmed by scanning electron microscopy (SEM) imaging of a dense, crack-free microstructure. At the nanoscale, Porcarello et al. (2024) reinforced biobased PG acrylic resins with CNTs for electroconductive, DLP-printed composites [13]. The lower-MW grade resin SA-TE 12 formed a denser network (crosslink density ≈ 10,994 mmol L^{-1}, T_g ≈ 53 °C) than SA-TE 60 (crosslink density ≈ 401 mmol L^{-1}, T_g ≈ −35 °C). CNTs maintained T_g, balancing UV-shielding with load transfer. Gelation times increased (~1 s to ~4 s) and curing slowed, but final stiffness was unaffected. CNTs induced shear-thinning beneficial for stress transfer and DLP printability. Field emission SEM revealed near-percolation CNT networks, enabling conductivity and sensing, consistent with the findings on SLA-printed multi-walled CNT-doped PG (meth)acrylate resins [62].

Multi-scale polymer-polymer architectures can merge macro- and microstructural reinforcement. Touré et al. (2020) integrated 3D printing of PCL-PGS blends with electrospinning [15]. The printed grid provided load-bearing support (modulus ≈ 102 MPa), while the electrospun mat increased stiffness to 250 ± 12 MPa through fiber bonding and reduced slippage. BG microparticles further raised stiffness to 311 ± 20 MPa at 10 wt%, though high loading reduced extensibility. The layered design distributed stresses, maintained geometry, and introduced bioactivity. After 56 days in PBS, mass loss was 10–15%; BG buffered acidic PGS degradation (pH ~6.0) and improved fibroblast viability (> 130% at day 2). Modulus declined over time due to porosity and matrix erosion.

Renewable-synthetic hybrids tailor sustainability and mechanics. Dos Santos et al. (2025) synthesized a 100% renewable glycerol–maleic anhydride-based acrylic polyester (PPH) blended with HEMA [82]. All resins had 97% biobased content. The formulation with 50% PPH exhibited the highest elongation (~130%), the 30% PPH formulation was stiffer, and the 70% PPH formulation was

Peer-reviewed version available at *Macromol* **2025**, *5*, 48; doi:https://doi.org/10.3390/macromol5040048

softer with reduced stability. T_g decreased with PPH (~60 °C to ~3 °C), while tensile strength remained 0.3–0.4 MPa, indicating stiffness changes arose from crosslink density. The semi-IPN structure formed due to faster HEMA polymerization and slower PPH conversion, producing interlaced phases that balanced flexibility and integrity.

5. 3D Printed Shape Memory PGs

Building on the earlier discussions of PG structure-property relationships, thermal stability, and mechanical reinforcement strategies, this section examines their application in shape memory systems. Shape memory polymers (SMPs) are smart materials capable of fixing a temporary shape and returning to their original configuration when stimulated by heat, light, or moisture [83]. PG-based SMPs leverage the tunable T_g, T_m, and crosslink density of PG to enable such responsive behavior. The polyhydroxyl backbone provides multiple reactive sites for chemical modification, such as acrylation [16,63], methacrylation [84], and urethane formation [85], forming covalent networks capable of recovering one or more programmed shapes upon sequential stimuli. This versatility supports applications ranging from soft actuators and adaptive biomedical devices to responsive packaging.

PG networks, whether pure or hybrid, exhibit high recovery and mechanical integrity during thermally induced shape changes. The shape-memory effect occurs at temperatures below or above the switching transition (T_{trans}), which corresponds to either T_g or T_m [86]. For example, PGD, with a T_m of 35–37 °C, enables body-temperature-triggered actuation for minimally invasive implants [87]. Extruded PGS elastomers achieve complete shape recovery within 10 s at 37 °C, and the incorporation of 30 wt% β-tricalcium phosphate preserves this rapid recovery [88]. Similarly, PGS-urethane-cellulose nanocomposites show excellent shape fixity (~98%) and recovery (~99%), with water-triggered actuation stabilizing within 30 min, making them well suited for cushioning and slow-release biomedical devices [85].

AM methods strongly influence SMP performance by enabling precise control over geometry and material structure. Both DLP and SLA produce high-resolution PG-based resins with well-defined recovery transitions. Thermal post-curing can further enhance crosslink density, improving recovery stress, shape recovery ratio (R_r), and shape fixity ratio (R_f). For example, acrylated PGD (APGD) transforms thermoset PGD into a UV-curable resin suitable for patient-specific devices [16]. By adjusting acrylation levels and prepolymer MW, researchers can tune thermal transitions (20–37 °C), crosslink density, and crystallinity to balance shape fixity, recovery speed, and compliance. An optimized high-MW, 18% APGD achieved shape fixity of ~97%, recovery of ~90%, and tensile properties compatible with soft tissue scaffolds without requiring organic solvents and while retaining physiologically relevant transitions. A recent example of functional integration is the DLP-based 4D printing of a biodegradable SMP copolymer, PGSA-PHEMA, for inferior vena cava filters (IVCFs) [78]. By controlling PGSA/PHEMA ratios, the transition temperature was precisely set at 37.8 °C for in vivo activation, while tensile strength exceeded 10 MPa. The printed IVCFs demonstrated high R_r (~92.9%), R_f (~97.3%), complete clot capture efficiency in flow models, gradual biodegradation (~10% mass loss over 8 weeks), and excellent biocompatibility both in vitro and in vivo.

These advances illustrate how combining SMP chemistry with precision AM enables deployable, patient-specific devices that maintain reliable performance under physiological conditions. The ability to tailor resin formulation, print resolution, and post-processing not only enhances shape-memory behavior but also broadens the scope of PG-based SMPs in biomedical and adaptive engineering applications.

6. Challenges and Opportunities

The versatility of polyglycerol (PG)-based systems in AM is offset by the absence of a fully integrated framework linking molecular design, processing parameters, and end-use performance. Although advances in thermal stability, mechanical reinforcement, and printability have been

Peer-reviewed version available at Macromol 2025, 5, 48; doi:https://doi.org/10.3390/macromol5040048

achieved, these improvements are often realized in isolation, limiting scalability and the ability to tailor materials for specific applications.

A major challenge lies in the incomplete mapping of structure-processing-property relationships. Variations in molecular architecture, curing dynamics, and AM build parameters can lead to unpredictable print fidelity and mechanical variability, especially in complex or large-scale parts. This issue is compounded by the lack of standardized AM-relevant testing protocols that capture anisotropy, interlayer adhesion, and fatigue behavior under realistic service conditions. Addressing this gap will require coupling high-throughput synthesis with machine learning-driven analysis to develop predictive formulation models that integrate resin chemistry, print parameters, and post-curing strategies [89].

Another critical barrier is the processing-performance tradeoff observed in UV-curable PG networks. Increasing crosslink density can improve tensile strength (to ~1.8 MPa) and thermal degradation resistance ($T_{5\%}$ > 350 °C) but often reduces flowability, layer resolution, and ductility (elongation at break frequently < 10%). Multi-network architectures, reactive diluents, and staged curing offer routes to decouple stiffness from printability, enabling high-strength parts without sacrificing resolution or flexibility [90].

Functional filler integration, essential for extending PG functionality into conductive, bioactive, or sensing domains, is hindered by dispersion challenges. Poor interfacial distribution at higher loadings can lead to agglomeration, stress concentrations, and reduced mechanical uniformity. Surface functionalization, in situ coupling, and hierarchical reinforcement strategies can mitigate these issues while maintaining processability [91].

Dimensional stability is limited by PG's predominantly amorphous nature, which restricts creep resistance and shape retention. Introducing semi-crystalline domains through blending with PEG or PCL can raise crystallinity (~20%) and T_m (> 50 °C), improving modulus and thermal stability [92]. However, excessive crystallinity can cause brittleness, underscoring the need for precise phase-morphology control via block copolymer design or targeted nucleation.

Finally, material optimization cycles remain slow, relying on sequential trial-and-error adjustments to chemistry, processing, and testing. This delays translation from laboratory-scale research to industrial deployment, especially for architectures requiring tight control over branching and functional group placement. Integrated design frameworks that co-optimize polymer synthesis, AM processability, and application-specific performance, supported by computational screening, could shorten development timelines, improve reproducibility, and expand PG adoption across sectors [93].

By addressing these interconnected challenges through coordinated advances in polymer design, processing optimization, and performance testing, PG-based systems can progress from niche research materials to industrially relevant AM platforms. The overall development pathway, capturing the relationship between molecular architecture, property enhancement strategies, application potential, and associated barriers, is summarized in Figure 2.

Peer-reviewed version available at *Macromol* **2025**, *5*, 48; doi:https://doi.org/10.3390/macromol5040048

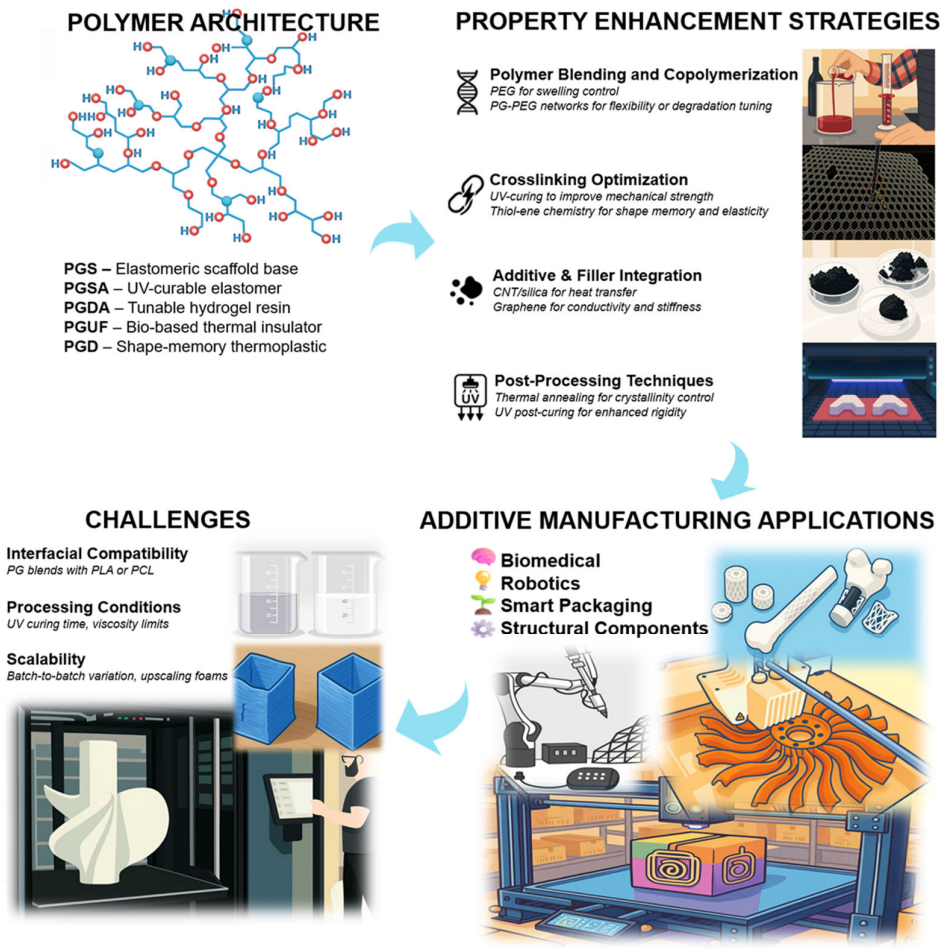

Figure 2. Development pathway of PG-based systems for AM, linking polymer architecture, property enhancement strategies, applications, and key challenges.

7. Conclusions

PG-based macromolecular systems are emerging as promising materials for AM, offering controllable thermal-mechanical performance suited to both biomedical and structural applications. Widespread adoption remains limited by gaps in understanding structure-processing-property relationships, challenges in achieving uniform filler dispersion, and trade-offs between performance and printability. Addressing these will require integrated approaches that combine molecular design, computational modeling, optimized AM workflows, and standardized performance evaluation. Future development should focus on sustainable synthesis routes, multifunctional material design, and predictive formulation strategies supported by high-throughput experimentation and data-driven tools. With coordinated advances across chemistry, processing, and application-driven testing, PG-based polymers could progress from niche research materials to industrially relevant platforms for high-performance, customizable, and sustainable manufacturing.

Author Contributions: Conceptualization; writing—review and editing, supervision: Reymark D. Maalihan; writing—original draft, review and editing: Julie Pearl M. Andal; writing—review and editing: Roxanne R. Navarro. All authors have read and agreed to the published version of the manuscript.

Peer-reviewed version available at *Macromol* **2025**, *5*, 48; doi:https://doi.org/10.3390/macromol5040048

Acknowledgments: J.P.M. Andal acknowledges the College of Engineering Technology – Graduate School, Batangas State University, Philippines for the technical support and access to research facilities that made this work possible.

Conflicts of Interest: The authors declare no conflicts of interest.

References

1. Sta. Agueda, J. R. H.; Chen, Q.; Maalihan, R. D.; Ren, J.; Da Silva, Í. G. M.; Dugos, N. P.; Caldona, E. B.; Advincula, R. C. 3D Printing of Biomedically Relevant Polymer Materials and Biocompatibility. *MRS Communications* **2021**, *11* (2), 197–212. https://doi.org/10.1557/s43579-021-00038-8.
2. Advincula, R. C.; Dizon, J. R. C.; Caldona, E. B.; Viers, R. A.; Siacor, F. D. C.; Maalihan, R. D.; Espera, A. H. On the Progress of 3D-Printed Hydrogels for Tissue Engineering. *MRS Communications* **2021**, *11* (5), 539–553. https://doi.org/10.1557/s43579-021-00069-1.
3. Maalihan, R. D.; Pajarito, B. B.; Advincula, R. C. 3D-Printing Methacrylate/Chitin Nanowhiskers Composites via Stereolithography: Mechanical and Thermal Properties. *Materials Today: Proceedings* **2020**, *33*, 1819–1824. https://doi.org/10.1016/j.matpr.2020.05.063.
4. Maalihan, R. D.; Pajarito, B. B.; Advincula, R. C. 3D-Printing Methacrylate/Chitin Nanowhiskers Composites via Stereolithography: Mechanical and Thermal Properties. *Materials Today: Proceedings* **2020**, *33*, 1819–1824. https://doi.org/10.1016/j.matpr.2020.05.063.
5. Bute, I.; Tarasovs, S.; Vidinejevs, S.; Vevere, L.; Sevcenko, J.; Aniskevich, A. Thermal Properties of 3D Printed Products from the Most Common Polymers. *Int J Adv Manuf Technol* **2023**, *124* (7–8), 2739–2753. https://doi.org/10.1007/s00170-022-10657-7.
6. Safai, L.; Cuellar, J. S.; Smit, G.; Zadpoor, A. A. A Review of the Fatigue Behavior of 3D Printed Polymers. *Additive Manufacturing* **2019**, *28*, 87–97. https://doi.org/10.1016/j.addma.2019.03.023.
7. Maalihan, R. D. Modelling the Toughness of Nanostructured Polyhedral Oligomeric Silsesquioxane Composites Fabricated by Stereolithography 3D Printing: A Response Surface Methodology and Artificial Neural Network Approach. *MSF* **2022**, *1053*, 41–46. https://doi.org/10.4028/p-6s4jp4.
8. Steyrer, B.; Neubauer, P.; Liska, R.; Stampfl, J. Visible Light Photoinitiator for 3D-Printing of Tough Methacrylate Resins. *Materials* **2017**, *10* (12), 1445. https://doi.org/10.3390/ma10121445.
9. Waidi, Y. O. Recent Advances in 4D-Printed Shape Memory Actuators. *Macromol. Rapid Commun.* **2025**, *46* (10). https://doi.org/10.1002/marc.202401141.
10. Liu, Y.-Y.; Intini, C.; Dobricic, M.; O'Brien, F. J.; LLorca, J.; Echeverry-Rendon, M. Collagen-Based 3D Printed Poly (Glycerol Sebacate) Composite Scaffold with Biomimicking Mechanical Properties for Enhanced Cartilage Defect Repair. *International Journal of Biological Macromolecules* **2024**, *280*, 135827. https://doi.org/10.1016/j.ijbiomac.2024.135827.
11. Wu, Z.; Jin, K.; Wang, L.; Fan, Y. A Review: Optimization for Poly(Glycerol Sebacate) and Fabrication Techniques for Its Centered Scaffolds. *Macromolecular Bioscience* **2021**, *21* (9). https://doi.org/10.1002/mabi.202100022.
12. Ao-Ieong, W.-S.; Chien, S.-T.; Jiang, W.-C.; Yet, S.-F.; Wang, J. The Effect of Heat Treatment toward Glycerol-Based, Photocurable Polymeric Scaffold: Mechanical, Degradation and Biocompatibility. *Polymers* **2021**, *13* (12), 1960. https://doi.org/10.3390/polym13121960.
13. Porcarello, M.; Bonardd, S.; Kortaberria, G.; Miyaji, Y.; Matsukawa, K.; Sangermano, M. 3D Printing of Electrically Conductive Objects with Biobased Polyglycerol Acrylic Monomers. *ACS Appl. Polym. Mater.* **2024**, *6* (5), 2868–2876. https://doi.org/10.1021/acsapm.3c03073.
14. Ruther, F.; Roether, J. A.; Boccaccini, A. R. 3D Printing of Mechanically Resistant Poly (Glycerol Sebacate) (PGS)-Zein Scaffolds for Potential Cardiac Tissue Engineering Applications. *Adv Eng Mater* **2022**, *24* (9), 2101768. https://doi.org/10.1002/adem.202101768.
15. Touré, A. B. R.; Mele, E.; Christie, J. K. Multi-Layer Scaffolds of Poly(Caprolactone), Poly(Glycerol Sebacate) and Bioactive Glasses Manufactured by Combined 3D Printing and Electrospinning. *Nanomaterials* **2020**, *10* (4), 626. https://doi.org/10.3390/nano10040626.

16. Akman, R.; Ramaraju, H.; Hollister, S. J. Development of Photocrosslinked Poly(Glycerol Dodecanedioate)—A Biodegradable Shape Memory Polymer for 3D-Printed Tissue Engineering Applications. *Adv Eng Mater* **2021**, *23* (10), 2100219. https://doi.org/10.1002/adem.202100219.
17. Godinho, B.; Nogueira, R.; Gama, N.; Ferreira, A. Synthesis and Characterization of Poly(Glycerol Sebacate), Poly(Glycerol Succinate) and Poly(Glycerol Sebacate-Co-Succinate). *J Polym Environ* **2024**, *32* (9), 4330–4347. https://doi.org/10.1007/s10924-024-03212-w.
18. Rosalia, M.; Rubes, D.; Serra, M.; Genta, I.; Dorati, R.; Conti, B. Polyglycerol Sebacate Elastomer: A Critical Overview of Synthetic Methods and Characterisation Techniques. *Polymers* **2024**, *16* (10), 1405. https://doi.org/10.3390/polym16101405.
19. Rafiee, Z.; Omidi, S. Modification of Carbon-Based Nanomaterials by Polyglycerol: Recent Advances and Applications. *RSC Adv.* **2022**, *12* (1), 181–192. https://doi.org/10.1039/d1ra07554c.
20. Pouyan, P.; Cherri, M.; Haag, R. Polyglycerols as Multi-Functional Platforms: Synthesis and Biomedical Applications. *Polymers* **2022**, *14* (13), 2684. https://doi.org/10.3390/polym14132684.
21. Osterwinter, C.; Schubert, C.; Tonhauser, C.; Wilms, D.; Frey, H.; Friedrich, C. Rheological Consequences of Hydrogen Bonding: Linear Viscoelastic Response of Linear Polyglycerol and Its Permethylated Analogues as a General Model for Hydroxyl-Functional Polymers. *Macromolecules* **2015**, *48* (1), 119–130. https://doi.org/10.1021/ma501674x.
22. Haag, R.; Sunder, A.; Stumbé, J.-F. An Approach to Glycerol Dendrimers and Pseudo-Dendritic Polyglycerols. *J. Am. Chem. Soc.* **2000**, *122* (12), 2954–2955. https://doi.org/10.1021/ja994363e.
23. Neumann, N.; Abels, G.; Koschek, K.; Boskamp, L. Crosslinked Hyperbranched Polyglycerol-Based Polymer Electrolytes for Lithium Metal Batteries. *Batteries* **2023**, *9* (9), 431. https://doi.org/10.3390/batteries9090431.
24. Yousefi Talouki, P.; Tamimi, R.; Zamanlui Benisi, S.; Goodarzi, V.; Shojaei, S.; Hesami Tackalou, S.; Samadikhah, H. R. Polyglycerol Sebacate (PGS)-Based Composite and Nanocomposites: Properties and Applications. *International Journal of Polymeric Materials and Polymeric Biomaterials* **2023**, *72* (17), 1360–1374. https://doi.org/10.1080/00914037.2022.2097681.
25. Goyal, S.; Hernández, N. B.; Cochran, E. W. An Update on the Future Prospects of Glycerol Polymers. *Polymer International* **2021**, *70* (7), 911–917. https://doi.org/10.1002/pi.6209.
26. Božič, M.; Majerič, M.; Denac, M.; Kokol, V. Mechanical and Barrier Properties of Soy Protein Isolate Films Plasticized with a Mixture of Glycerol and Dendritic Polyglycerol. *J of Applied Polymer Sci* **2015**, *132* (17). https://doi.org/10.1002/app.41837.
27. Nakiou, E. A.; Lazaridou, M.; Pouroutzidou, G. K.; Michopoulou, A.; Tsamesidis, I.; Liverani, L.; Arango-Ospina, M.; Beketova, A.; Boccaccini, A. R.; Kontonasaki, E.; Bikiaris, D. N. Poly(Glycerol Succinate) as Coating Material for 1393 Bioactive Glass Porous Scaffolds for Tissue Engineering Applications. *Polymers* **2022**, *14* (22), 5028. https://doi.org/10.3390/polym14225028.
28. Sunder, A.; Hanselmann, R.; Frey, H.; Mülhaupt, R. Controlled Synthesis of Hyperbranched Polyglycerols by Ring-Opening Multibranching Polymerization. *Macromolecules* **1999**, *32* (13), 4240–4246. https://doi.org/10.1021/ma990090w.
29. Thomas, A.; Müller, S. S.; Frey, H. Beyond Poly(Ethylene Glycol): Linear Polyglycerol as a Multifunctional Polyether for Biomedical and Pharmaceutical Applications. *Biomacromolecules* **2014**, *15* (6), 1935–1954. https://doi.org/10.1021/bm5002608.
30. Abbina, S.; Vappala, S.; Kumar, P.; Siren, E. M. J.; La, C. C.; Abbasi, U.; Brooks, D. E.; Kizhakkedathu, J. N. Hyperbranched Polyglycerols: Recent Advances in Synthesis, Biocompatibility and Biomedical Applications. *J. Mater. Chem. B* **2017**, *5* (47), 9249–9277. https://doi.org/10.1039/C7TB02515G.
31. Dey, P.; Hemmati-Sadeghi, S.; Haag, R. Hydrolytically Degradable, Dendritic Polyglycerol Sulfate Based Injectable Hydrogels Using Strain Promoted Azide–Alkyne Cycloaddition Reaction. *Polym. Chem.* **2016**, *7* (2), 375–383. https://doi.org/10.1039/C5PY01326G.
32. Moncalvo, F.; Lacroce, E.; Franzoni, G.; Altomare, A.; Fasoli, E.; Aldini, G.; Sacchetti, A.; Cellesi, F. Selective Protein Conjugation of Poly(Glycerol Monomethacrylate) and Poly(Polyethylene Glycol Methacrylate) with Tunable Topology via Reductive Amination with Multifunctional ATRP Initiators for Activity Preservation. *Macromolecules* **2022**, *55* (17), 7454–7468. https://doi.org/10.1021/acs.macromol.2c00783.

33. Ye, H.; Owh, C.; Loh, X. J. A Thixotropic Polyglycerol Sebacate-Based Supramolecular Hydrogel Showing UCST Behavior. *RSC Adv.* **2015**, *5* (60), 48720–48728. https://doi.org/10.1039/c5ra08222f.
34. Leite, D. B. C.; De Moura, E. M.; Muniz, E. C.; Da Silva Filho, E. C.; Mendes, A. N.; Filgueiras, L. A.; De Abreu Júnior, A. R.; Gonçalves, J. C. R.; Marques, K. K. G.; Sobral, M. V.; Carvalho, A. L. M.; De Moura, C. V. R. Synthesis of Polyglycerol/PolyCaprolactone Nanocopolymers as Innovative Architectures for Drug Delivery. *BioNanoSci.* **2024**, *14* (3), 2829–2841. https://doi.org/10.1007/s12668-024-01557-z.
35. Taresco, V.; Suksiriworapong, J.; Creasey, R.; Burley, J. C.; Mantovani, G.; Alexander, C.; Treacher, K.; Booth, J.; Garnett, M. C. Properties of Acyl Modified Poly(Glycerol-Adipate) Comb-like Polymers and Their Self-Assembly into Nanoparticles. *J. Polym. Sci. Part A: Polym. Chem.* **2016**, *54* (20), 3267–3278. https://doi.org/10.1002/pola.28215.
36. Pin, J.-M.; Valerio, O.; Misra, M.; Mohanty, A. Impact of Butyl Glycidyl Ether Comonomer on Poly(Glycerol–Succinate) Architecture and Dynamics for Multifunctional Hyperbranched Polymer Design. *Macromolecules* **2017**, *50* (3), 732–745. https://doi.org/10.1021/acs.macromol.6b02424.
37. Miceli, E.; Wedepohl, S.; Osorio Blanco, E. R.; Rimondino, G. N.; Martinelli, M.; Strumia, M.; Molina, M.; Kar, M.; Calderón, M. Semi-Interpenetrated, Dendritic, Dual-Responsive Nanogels with Cytochrome c Corona Induce Controlled Apoptosis in HeLa Cells. *European Journal of Pharmaceutics and Biopharmaceutics* **2018**, *130*, 115–122. https://doi.org/10.1016/j.ejpb.2018.06.023.
38. Janiszewska, N.; Basinska, T.; Gadzinowski, M.; Slomkowski, S.; Makowski, T.; Awsiuk, K. Impact of Polyglycidol Block Architecture in Polystyrene-b-Polyglycidol Copolymers on the Properties of Thin Films and Protein Adsorption. *Applied Surface Science* **2024**, *669*, 160458. https://doi.org/10.1016/j.apsusc.2024.160458.
39. Son, S.; Park, H.; Shin, E.; Shibasaki, Y.; Kim, B. Architecture-controlled Synthesis of Redox-degradable Hyperbranched Polyglycerol Block Copolymers and the Structural Implications of Their Degradation. *J. Polym. Sci. Part A: Polym. Chem.* **2016**, *54* (12), 1752–1761. https://doi.org/10.1002/pola.28031.
40. Cherri, M.; Romero, J. F.; Steiner, L.; Dimde, M.; Koeppe, H.; Paulus, B.; Mohammadifar, E.; Haag, R. Power of the Disulfide Bond: An Ideal Random Copolymerization of Biodegradable Redox-Responsive Hyperbranched Polyglycerols. *Biomacromolecules* **2024**, *25* (1), 119–133. https://doi.org/10.1021/acs.biomac.3c00863.
41. Domalanta, M. R. B.; Ali, M. R. R.; Maalihan, R. D.; Caldona, E. B. Mechanistic Effects of HFP Content on the Surface Structure and Protective Action of PVDF-HFP Coatings. *Progress in Organic Coatings* **2025**, *198*, 108879. https://doi.org/10.1016/j.porgcoat.2024.108879.
42. Dahlgren, J.; Stafslien, S. J.; Vanderwal, L.; Bahr, J.; Allen, P.; Finlay, J. A.; Clare, A. S.; Webster, D. C. Investigation of Amphiphilic PDMS-Hyperbranched Polyglycerol Copolymers to Tune the Fouling-Release Properties in a Moisture Curable Coating System. *Langmuir* **2025**, *41* (5), 3377–3391. https://doi.org/10.1021/acs.langmuir.4c04338.
43. Schubert, C.; Schömer, M.; Steube, M.; Decker, S.; Friedrich, C.; Frey, H. Systematic Variation of the Degree of Branching (DB) of Polyglycerol via Oxyanionic Copolymerization of Glycidol with a Protected Glycidyl Ether and Its Impact on Rheological Properties. *Macro Chemistry & Physics* **2018**, *219* (1). https://doi.org/10.1002/macp.201700376.
44. Junge, F.; Haag, R. Effect of Fluorophilic- and Hydrophobic-Modified Polyglycerol-Based Coatings on the Wettability of Low Surface Energy Polymers. *Langmuir* **2025**, *41* (5), 3305–3314. https://doi.org/10.1021/acs.langmuir.4c04220.
45. Godinho, B.; Gama, N.; Ferreira, A. Different Methods of Synthesizing Poly(Glycerol Sebacate) (PGS): A Review. *Front. Bioeng. Biotechnol.* **2022**, *10*. https://doi.org/10.3389/fbioe.2022.1033827.
46. Balser, S.; Zhao, Z.; Zharnikov, M.; Terfort, A. Effect of the Crosslinking Agent on the Biorepulsive and Mechanical Properties of Polyglycerol Membranes. *Colloids and Surfaces B: Biointerfaces* **2023**, *225*, 113271. https://doi.org/10.1016/j.colsurfb.2023.113271.
47. Valerio, O.; Misra, M.; Mohanty, A. K. Poly(Glycerol-*Co*-Diacids) Polyesters: From Glycerol Biorefinery to Sustainable Engineering Applications, A Review. *ACS Sustainable Chem. Eng.* **2018**, *6* (5), 5681–5693. https://doi.org/10.1021/acssuschemeng.7b04837.
48. Schubert, C.; Dreier, P.; Nguyen, T.; Maciol, K.; Blankenburg, J.; Friedrich, C.; Frey, H. Synthesis of Linear Polyglycerols with Tailored Degree of Methylation by Copolymerization and the Effect on Thermorheological Behavior. *Polymer* **2017**, *121*, 328–339. https://doi.org/10.1016/j.polymer.2017.05.030.

49. Saudi, A.; Zebarjad, S. M.; Salehi, H.; Katoueizadeh, E.; Alizadeh, A. Assessing Physicochemical, Mechanical, and in Vitro Biological Properties of Polycaprolactone/Poly(Glycerol Sebacate)/Hydroxyapatite Composite Scaffold for Nerve Tissue Engineering. *Materials Chemistry and Physics* **2022**, *275*, 125224. https://doi.org/10.1016/j.matchemphys.2021.125224.
50. Jafari, M.; Abolmaali, S. S.; Borandeh, S.; Najafi, H.; Zareshahrabadi, Z.; Koohi-Hosseinabadi, O.; Azarpira, N.; Zomorodian, K.; Tamaddon, A. M. Dendritic Hybrid Materials Comprising Polyhedral Oligomeric Silsesquioxane (POSS) and Hyperbranched Polyglycerol for Effective Antifungal Drug Delivery and Therapy in Systemic Candidiasis. *Nanoscale* **2023**, *15* (39), 16163–16177. https://doi.org/10.1039/d3nr04321e.
51. Phetnoi, N.; Amornkitbamrung, L.; Charoensuk, K.; Sapcharoenkun, C.; Jubsilp, C.; Ekgasit, S.; Rimdusit, S. Fast Magnetic-Responsive Shape Memory Composites from Bio-Based Benzoxazine/Polyglycerol Polyglycidyl Ether Copolymers Highly Filled with Iron Oxide Nanoparticles. *Composites Part A: Applied Science and Manufacturing* **2024**, *186*, 108398. https://doi.org/10.1016/j.compositesa.2024.108398.
52. Risley, B. B.; Ding, X.; Chen, Y.; Miller, P. G.; Wang, Y. Citrate Crosslinked Poly(Glycerol Sebacate) with Tunable Elastomeric Properties. *Macromolecular Bioscience* **2021**, *21* (2). https://doi.org/10.1002/mabi.202000301.
53. Golbaten-Mofrad, H.; Salehi, M. H.; Jafari, S. H.; Goodarzi, V.; Entezari, M.; Hashemi, M. Preparation and Properties Investigation of Biodegradable Poly (Glycerol Sebacate-*Co*-gelatin) Containing Nanoclay and Graphene Oxide for Soft Tissue Engineering Applications. *J Biomed Mater Res* **2022**, *110* (10), 2241–2257. https://doi.org/10.1002/jbm.b.35073.
54. Jaberi, N.; Fakhri, V.; Zeraatkar, A.; Jafari, A.; Uzun, L.; Shojaei, S.; Asefnejad, A.; Faghihi Rezaei, V.; Goodarzi, V.; Su, C.; Ghaffarian Anbaran, S. R. Preparation and Characterization of a New Bio Nanocomposites Based Poly(Glycerol Sebacic-urethane) Containing Nano-clay (Cloisite Na^+) and Its Potential Application for Tissue Engineering. *J Biomed Mater Res* **2022**, *110* (10), 2217–2230. https://doi.org/10.1002/jbm.b.35071.
55. Kasza, G.; Stumphauser, T.; Nádor, A.; Osváth, Z.; Szarka, G.; Domján, A.; Mosnáček, J.; Iván, B. Hyperbranched Polyglycerol Nanoparticles Based Multifunctional, Nonmigrating Hindered Phenolic Macromolecular Antioxidants: Synthesis, Characterization and Its Stabilization Effect on Poly(Vinyl Chloride). *Polymer* **2017**, *124*, 210–218. https://doi.org/10.1016/j.polymer.2017.07.061.
56. Schlaich, C.; Wei, Q.; Haag, R. Mussel-Inspired Polyglycerol Coatings with Controlled Wettability: From Superhydrophilic to Superhydrophobic Surface Coatings. *Langmuir* **2017**, *33* (38), 9508–9520. https://doi.org/10.1021/acs.langmuir.7b01291.
57. Tevlek, A.; Agacik, D. T.; Aydin, H. M. Stretchable Poly(Glycerol-sebacate)/B-tricalcium Phosphate Composites with Shape Recovery Feature by Extrusion. *J of Applied Polymer Sci* **2020**, *137* (20). https://doi.org/10.1002/app.48689.
58. You, A.; Kim, J.; Ryu, S. Synthesis of Acrylate-Functionalized Polyglycerols and an Investigation of Their UV Curing Behaviors. *ChemistrySelect* **2023**, *8* (3). https://doi.org/10.1002/slct.202203859.
59. Barra, G.; Guadagno, L.; Raimondo, M.; Santonicola, M. G.; Toto, E.; Vecchio Ciprioti, S. A Comprehensive Review on the Thermal Stability Assessment of Polymers and Composites for Aeronautics and Space Applications. *Polymers* **2023**, *15* (18), 3786. https://doi.org/10.3390/polym15183786.
60. Kroll, D. M.; Croll, S. G. Influence of Crosslinking Functionality, Temperature and Conversion on Heterogeneities in Polymer Networks. *Polymer* **2015**, *79*, 82–90. https://doi.org/10.1016/j.polymer.2015.10.020.
61. Hu, G.; Cao, Z.; Hopkins, M.; Lyons, J. G.; Brennan-Fournet, M.; Devine, D. M. Nanofillers Can Be Used to Enhance the Thermal Conductivity of Commercially Available SLA Resins. *Procedia Manufacturing* **2019**, *38*, 1236–1243. https://doi.org/10.1016/j.promfg.2020.01.215.
62. Krumins, E.; George, K.; Taresco, V.; Sun, X.; Hoggett, S.; Duncan, J.; Cuzzucoli Crucitti, V.; Segal, J.; Irvine, D. J.; Khlobystov, A.; Wildman, R. Sustainable and Electrically Conductive Poly(Glycerol) (Meth)Acrylate Resins for Stereolithography and Volumetric Additive Manufacturing. In *Smart Materials for Opto-Electronic Applications 2025*; Rendina, I., Petti, L., Sagnelli, D., Nenna, G., Eds.; SPIE: Prague, Czech Republic, 2025; p 32. https://doi.org/10.1117/12.3056326.
63. Akman, R.; Ramaraju, H.; Hollister, M.; Verga, A.; Hollister, S. J. Thermal Post-Processing of 3D-Printed Poly(Glycerol Dodecanedioate) Controls Mechanics and Shape Memory Properties. *Polymer Science & Technology* **2025**, *1* (2), 132–143. https://doi.org/10.1021/polymscitech.5c00012.

64. Ao-Ieong, W.-S.; Chien, S.-T.; Jiang, W.-C.; Yet, S.-F.; Wang, J. The Effect of Heat Treatment toward Glycerol-Based, Photocurable Polymeric Scaffold: Mechanical, Degradation and Biocompatibility. *Polymers* **2021**, *13* (12), 1960. https://doi.org/10.3390/polym13121960.
65. Liu, Q.; Tian, M.; Ding, T.; Shi, R.; Feng, Y.; Zhang, L.; Chen, D.; Tian, W. Preparation and Characterization of a Thermoplastic Poly(Glycerol Sebacate) Elastomer by Two-step Method. *J of Applied Polymer Sci* **2007**, *103* (3), 1412–1419. https://doi.org/10.1002/app.24394.
66. Abdullah, T.; Gzara, L.; Simonetti, G.; Alshahrie, A.; Salah, N.; Morganti, P.; Chianese, A.; Fallahi, A.; Tamayol, A.; Bencherif, S.; Memic, A. The Effect of Poly (Glycerol Sebacate) Incorporation within Hybrid Chitin–Lignin Sol–Gel Nanofibrous Scaffolds. *Materials* **2018**, *11* (3), 451. https://doi.org/10.3390/ma11030451.
67. Mohammadbagheri, Z.; Rahmati, A.; Saeedi, S.; Movahedi, B. Bio-Based Nanocomposite Hydrogels Derived from Poly (Glycerol Tartrate) and Cellulose: Thermally Stable and Green Adsorbents for Efficient Adsorption of Heavy Metals. *Chemosphere* **2024**, *349*, 140956. https://doi.org/10.1016/j.chemosphere.2023.140956.
68. Hevilla, V.; Sonseca, Á.; Fernández-García, M. Straightforward Enzymatic Methacrylation of Poly(Glycerol Adipate) for Potential Applications as UV Curing Systems. *Polymers* **2023**, *15* (14), 3050. https://doi.org/10.3390/polym15143050.
69. Calderon, M. J. P.; Dumancas, G. G.; Gutierrez, C. S.; Lubguban, A. A.; Alguno, A. C.; Malaluan, R. M.; Lubguban, A. A. Producing Polyglycerol Polyester Polyol for Thermoplastic Polyurethane Application: A Novel Valorization of Glycerol, a by-Product of Biodiesel Production. *Heliyon* **2023**, *9* (9), e19491. https://doi.org/10.1016/j.heliyon.2023.e19491.
70. Ramaraju, H.; Solorio, L. D.; Bocks, M. L.; Hollister, S. J. Degradation Properties of a Biodegradable Shape Memory Elastomer, Poly(Glycerol Dodecanoate), for Soft Tissue Repair. *PLoS ONE* **2020**, *15* (2), e0229112. https://doi.org/10.1371/journal.pone.0229112.
71. Han, J.; Hong, J.; Choi, C.; Cha, C. Physicochemically Tunable Hyperbranched Polyglycerol Copolymerized with Functional Aziridine As a Versatile, Multivalent Cross-Linker for Waterborne Acrylic Adhesives. *ACS Appl. Polym. Mater.* **2024**, *6* (18), 11167–11179. https://doi.org/10.1021/acsapm.4c01502.
72. Maalihan, R. D.; Briones, L. I. B.; Canarias, E. P.; Lanuza, G. P. On the 3D Printing and Flame Retardancy of Expandable Graphite-Coated Polylactic Acid. *Materials Today: Proceedings* **2023**, S2214785323048125. https://doi.org/10.1016/j.matpr.2023.09.140.
73. Alcantara, K. C.; Lucido, K. V.; Mabilangan, K. H. R.; Magsino, R. M. L. V.; Aquino, A. P.; Sangalang, R. H.; Maalihan, R. D. Copper Removal with Zeolite/Polylactic Acid Beads: Neural Networks and Fixed-Bed Column Insights. *Chem Eng & Technol* **2025**, *48* (5), e70024. https://doi.org/10.1002/ceat.70024.
74. Ji, S.; Stricher, M.; Nadaud, F.; Guenin, E.; Egles, C.; Delbecq, F. Solvent-Free Production by Extrusion of Bio-Based Poly(Glycerol-Co-Diacids) Sheets for the Development of Biocompatible and Electroconductive Elastomer Composites. *Polymers* **2022**, *14* (18), 3829. https://doi.org/10.3390/polym14183829.
75. Aleemardani, M.; Johnson, L.; Trikić, M. Z.; Green, N. H.; Claeyssens, F. Synthesis and Characterisation of Photocurable Poly(Glycerol Sebacate)-Co-Poly(Ethylene Glycol) Methacrylates. *Materials Today Advances* **2023**, *19*, 100410. https://doi.org/10.1016/j.mtadv.2023.100410.
76. Yeh, Y.-C.; Ouyang, L.; Highley, C. B.; Burdick, J. A. Norbornene-Modified Poly(Glycerol Sebacate) as a Photocurable and Biodegradable Elastomer. *Polym. Chem.* **2017**, *8* (34), 5091–5099. https://doi.org/10.1039/C7PY00323D.
77. Ravi, P.; Wright, J.; Shiakolas, P. S.; Welch, T. R. Three-Dimensional Printing of Poly(Glycerol Sebacate Fumarate) Gadodiamide-Poly(Ethylene Glycol) Diacrylate Structures and Characterization of Mechanical Properties for Soft Tissue Applications. *Journal of Biomedical Materials Research Part B: Applied Biomaterials* **2019**, *107* (3), 664–671. https://doi.org/10.1002/jbm.b.34159.
78. Qu, R.; Zhou, D.; Guo, T.; He, W.; Cui, C.; Zhou, Y.; Zhang, Y.; Tang, Z.; Zhang, X.; Wang, Q.; Wang, T.; Zhang, Y. 4D Printing of Shape Memory Inferior Vena Cava Filters Based on Copolymer of Poly(Glycerol Sebacate) Acrylate-*Co*-Hydroxyethyl Methacrylate (PGSA-HEMA). *Materials & Design* **2023**, *225*, 111556. https://doi.org/10.1016/j.matdes.2022.111556.
79. Maalihan, R. D.; Aggari, J. C. V.; Alon, A. S.; Latayan, R. B.; Montalbo, F. J. P.; Javier, A. D. On the Optimized Fused Filament Fabrication of Polylactic Acid Using Multiresponse Central Composite Design and Desirability

Function Algorithm. *Proceedings of the Institution of Mechanical Engineers, Part E: Journal of Process Mechanical Engineering* **2024**, 09544089241247454. https://doi.org/10.1177/09544089241247454.

80. Gürbüz, B.; Baran, E. T.; Tahmasebifar, A.; Yilmaz, B. Construction of Aligned Polycaprolactone/Poly(Glycerol Sebacate)/Polysulfone Nanofibrous Scaffolds for Tissue Engineering of the Ventricularis Layer of Heart Valves. *Polymers for Advanced Techs* **2024**, *35* (11), e6629. https://doi.org/10.1002/pat.6629.
81. Yang, Z.; Zhang, X.; Liu, X.; Guan, X.; Zhang, C.; Niu, Y. Polyglycerol-Based Organic-Inorganic Hybrid Adhesive with High Early Strength. *Materials & Design* **2017**, *117*, 1–6. https://doi.org/10.1016/j.matdes.2016.12.069.
82. Dos Santos, G. I.; Gaglieri, C.; Alarcon, R. T.; De Moura, A.; Dos Santos, F. B.; Bannach, G. Glycerol and Maleic Anhydride-Based Acrylic Polyester: A Solution for Greener Photocurable Resins for 3D Printing of Renewable Materials. *ACS Sustainable Chem. Eng.* **2025**, *13* (25), 9771–9782. https://doi.org/10.1021/acssuschemeng.5c03006.
83. Zulkifli, Z.; Tan, J. J.; Ku Marsilla, K. I.; Rusli, A.; Abdullah, M. K.; Shuib, R. K.; Shafiq, M. D.; Abdul Hamid, Z. A. Shape Memory Poly (Glycerol Sebacate)-Based Electrospun Fiber Scaffolds for Tissue Engineering Applications: A Review. *Journal of Applied Polymer Science* **2022**, *139* (22), 52272. https://doi.org/10.1002/app.52272.
84. Ramaraju, H.; McAtee, A. M.; Akman, R. E.; Verga, A. S.; Bocks, M. L.; Hollister, S. J. Sterilization Effects on Poly(Glycerol Dodecanedioate): A Biodegradable Shape Memory Elastomer for Biomedical Applications. *J Biomed Mater Res* **2023**, *111* (4), 958–970. https://doi.org/10.1002/jbm.b.35205.
85. Wu, T.; Frydrych, M.; O'Kelly, K.; Chen, B. Poly(Glycerol Sebacate Urethane)–Cellulose Nanocomposites with Water-Active Shape-Memory Effects. *Biomacromolecules* **2014**, *15* (7), 2663–2671. https://doi.org/10.1021/bm500507z.
86. Cai, W.; Liu, L. Shape-Memory Effect of Poly (Glycerol–Sebacate) Elastomer. *Materials Letters* **2008**, *62* (14), 2171–2173. https://doi.org/10.1016/j.matlet.2007.11.042.
87. Ramaraju, H.; Massarella, D.; Wong, C.; Verga, A. S.; Kish, E. C.; Bocks, M. L.; Hollister, S. J. Percutaneous Delivery and Degradation of a Shape Memory Elastomer Poly(Glycerol Dodecanedioate) in Porcine Pulmonary Arteries. *Biomaterials* **2023**, *293*, 121950. https://doi.org/10.1016/j.biomaterials.2022.121950.
88. Tevlek, A.; Agacik, D. T.; Aydin, H. M. Stretchable Poly(Glycerol-Sebacate)/β-Tricalcium Phosphate Composites with Shape Recovery Feature by Extrusion. *Journal of Applied Polymer Science* **2020**, *137* (20), 48689. https://doi.org/10.1002/app.48689.
89. Gokcekuyu, Y.; Ekinci, F.; Guzel, M. S.; Acici, K.; Aydin, S.; Asuroglu, T. Artificial Intelligence in Biomaterials: A Comprehensive Review. *Applied Sciences* **2024**, *14* (15), 6590. https://doi.org/10.3390/app14156590.
90. Timofticiuc, I.-A.; Călinescu, O.; Iftime, A.; Dragosloveanu, S.; Caruntu, A.; Scheau, A.-E.; Badarau, I. A.; Didilescu, A. C.; Caruntu, C.; Scheau, C. Biomaterials Adapted to Vat Photopolymerization in 3D Printing: Characteristics and Medical Applications. *Journal of Functional Biomaterials* **2024**, *15* (1), 7. https://doi.org/10.3390/jfb15010007.
91. Jiang, P.; Ji, Z.; Wang, X.; Zhou, F. Surface Functionalization – a New Functional Dimension Added to 3D Printing. *J. Mater. Chem. C* **2020**, *8* (36), 12380–12411. https://doi.org/10.1039/D0TC02850A.
92. Delaey, J.; Dubruel, P.; Van Vlierberghe, S. Shape-Memory Polymers for Biomedical Applications. *Advanced Functional Materials* **2020**, *30* (44), 1909047. https://doi.org/10.1002/adfm.201909047.
93. Zhang, S.; Vijayavenkataraman, S.; Lu, W. F.; Fuh, J. Y. H. A Review on the Use of Computational Methods to Characterize, Design, and Optimize Tissue Engineering Scaffolds, with a Potential in 3D Printing Fabrication. *Journal of Biomedical Materials Research Part B: Applied Biomaterials* **2019**, *107* (5), 1329–1351. https://doi.org/10.1002/jbm.b.34226.